

Rapid hepatic clearance of ^{99m}Tc -TMEOP: a new candidate for myocardial perfusion imaging

Lode R. Goethals^{a,b*}, Isabel Santos^c, Vicky Caveliers^{b,d}, Antonio Paulo^c, Frank De Geeter^b, Patrício G. Lurdes^c, Célia Fernandes^c and Tony Lahoutte^{b,d}

Background: ^{99m}Tc labeled radiotracers used in clinical practice lack the perfect characteristics for myocardial perfusion imaging. In particular, the high liver uptake can interfere in the interpretation of the inferior myocardial wall. Within the tricarbonyl approach, we used tris(pyrazolyl)methane ^{99m}Tc organometallic complexes as a lead structure. Herein we present the production, *in vivo* and *in vitro* metabolic studies in rats and the first *in vivo* biodistribution in rats for tri-methoxy-tris-pyrazolyl- $^{99m}\text{Tc}(\text{CO})_3$ (^{99m}Tc -TMEOP), compared with ^{99m}Tc -sestamibi and ^{99m}Tc -tetrofosmin. **Methods:** The chemical identity of ^{99m}Tc -TMEOP was characterized by RP-HPLC. The octanol–water partition coefficient was determined under physiological conditions. *In vitro* stability and protein binding were determined using RP-HPLC. *In vivo* stability was determined in blood, heart, liver and kidney homogenates, intestine and urine using RP-HPLC. *In vivo* biodistribution was determined using dynamic planar acquisitions. Pinhole gated SPECT images were performed in other animals. Cardiac, liver and lung uptake were expressed as differential uptake ratios by drawing regions of interest in the organs of interest and around the total body. Heart–liver and heart–lung ratios were derived. Cardiac uptake was also expressed as percentage of injected activity. SPECT images were processed to determine the heart–liver ratio on SPECT images, to compare functional parameters between different tracers and to visualize homogeneous intracardiac tracer distribution. **Results:** ^{99m}Tc -TMEOP is a moderately lipophilic cation, is stable and does not undergo any transformation *in vitro*. ^{99m}Tc -TMEOP also shows a high *in vivo* stability. *In vivo* imaging shows liver kinetics faster than those of ^{99m}Tc -sestamibi and ^{99m}Tc -tetrofosmin. Cardiac uptake and functional analysis of pinhole gated SPECT data are comparable to those of ^{99m}Tc -sestamibi and ^{99m}Tc -tetrofosmin. **Conclusion:** Although ^{99m}Tc -TMEOP shows a cardiac uptake between those of ^{99m}Tc -sestamibi and ^{99m}Tc -tetrofosmin, a better heart–liver ratio is obtained due to the faster liver washout. These results suggest possible faster cardiac perfusion imaging using ^{99m}Tc -TMEOP without liver activity interference. Copyright © 2010 John Wiley & Sons, Ltd.

Keywords: myocardial perfusion imaging; tracer development; small animal; heart–liver ratio, biodistribution

1. INTRODUCTION

^{99m}Tc labeled radiotracers, such as ^{99m}Tc -sestamibi and ^{99m}Tc -tetrofosmin are widely used for myocardial perfusion imaging (1–3). However, both ^{99m}Tc -sestamibi and ^{99m}Tc -tetrofosmin are not ideal myocardial perfusion imaging agents. Normal liver uptake interferes with the analysis of the inferior wall of the left ventricle and their flow–extraction rates decrease at higher flow rates (4–11). This ‘roll-off’ phenomenon in flow–extraction limits the sensitivity of a tracer to detect coronary artery disease and reversible perfusion defects by reducing defect contrast and affects the detection of mild rather than severe coronary artery disease (10–13). The increased liver uptake, however, leads to clinically significant false positive or negative reporting of myocardial ischemia. Photons originating from the liver scatter in the inferior wall, resulting in an apparently increased uptake in the myocardium. This is confusing when comparing rest and stress studies. In general, liver uptake is higher in rest studies, resulting in a relatively higher inferior wall uptake compared with stress studies and the possibility of false diagnosis of inferior wall ischemia (14). These patients are then

incorrectly referred to coronary angiography. Where the liver uptake is relatively high in stress compared with rest studies, relatively important myocardial ischemia can be missed in the inferior wall. Stimulating patients to eat fatty food prior to

* Correspondence to: L. R. Goethals, Department of Radiology, Laarbeeklaan 101, 1090 Brussels, Belgium.
E-mail: Lode.Goethals@vub.ac.be

a L. R. Goethals
Department of Radiology, University Hospital Brussels (UZ Brussel), Brussels, Belgium

b L. R. Goethals, V. Caveliers, F. De Geeter, T. Lahoutte
In Vivo Cellular and Molecular Imaging (ICMI) laboratory, Vrije Universiteit Brussel (VUB), Brussels, Belgium

c I. Santos, A. Paulo, P. G. Lurdes, C. Fernandes, P. G. Lurdes, C. Fernandes
Unidade Ciências Químicas e Radiofarmacêuticas, Instituto Tecnológico e Nuclear, Sacavém, Portugal

d V. Caveliers, T. Lahoutte
Department of Nuclear Medicine, University Hospital Brussels (UZ Brussel), Brussels, Belgium

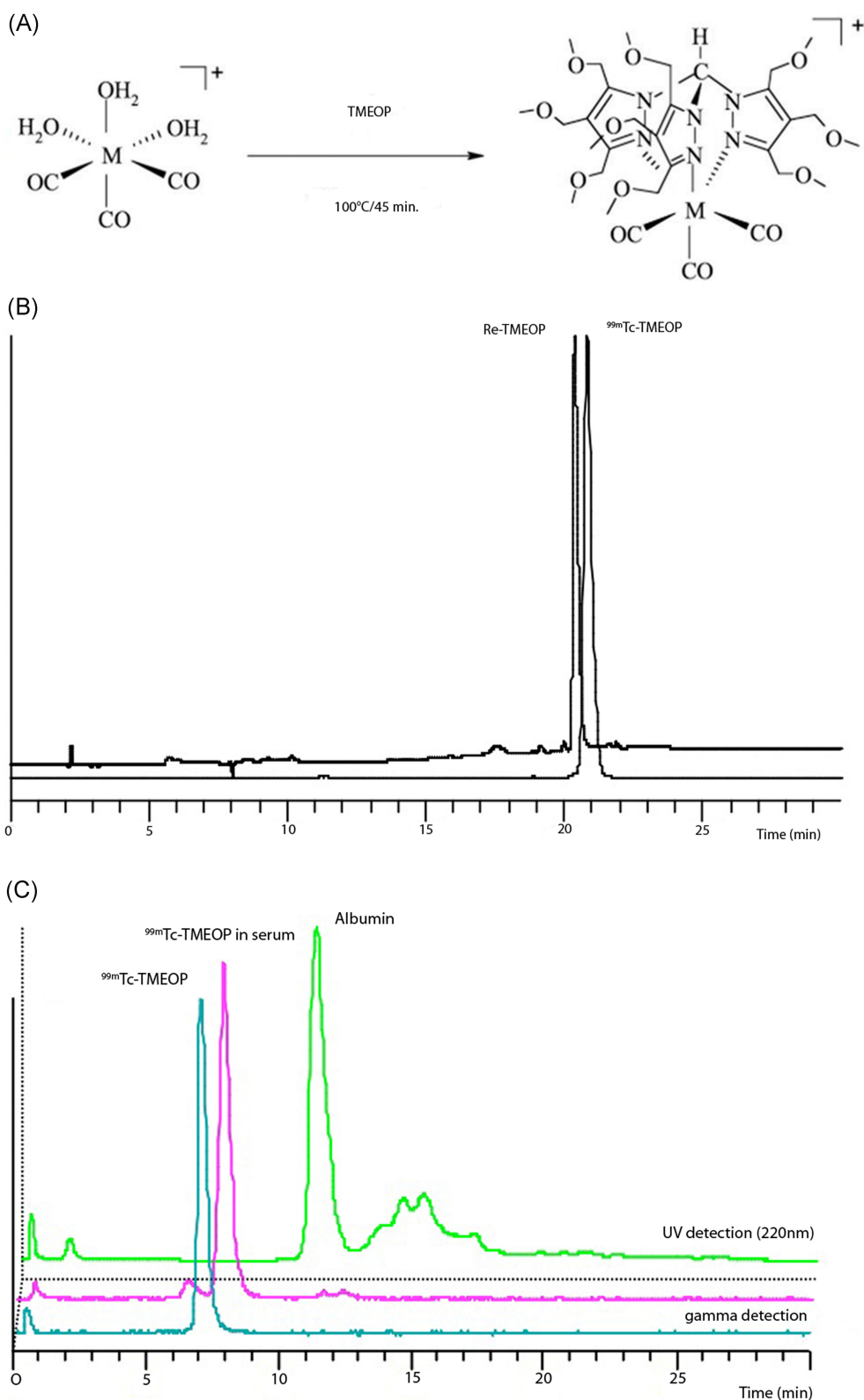


Figure 1. (A) Synthesis and chemical structure of ^{99m}Tc-TMEOP. (B) HPLC chromatogram of ^{99m}Tc-TMEOP and Re-TMEOP. (C) HPLC profiles of ^{99m}Tc-TMEOP in the labeling conditions (blue)(gamma detection); ^{99m}Tc-TMEOP after incubation with human serum at 37 °C for 2 h (gamma and UV detection is shown by pink and green profiles, respectively). (D) Radioactive HPLC profiles of ^{99m}Tc-TMEOP in comparison with the HPLC profiles of the radioactivity extracted from rat tissues at 1h post injection.

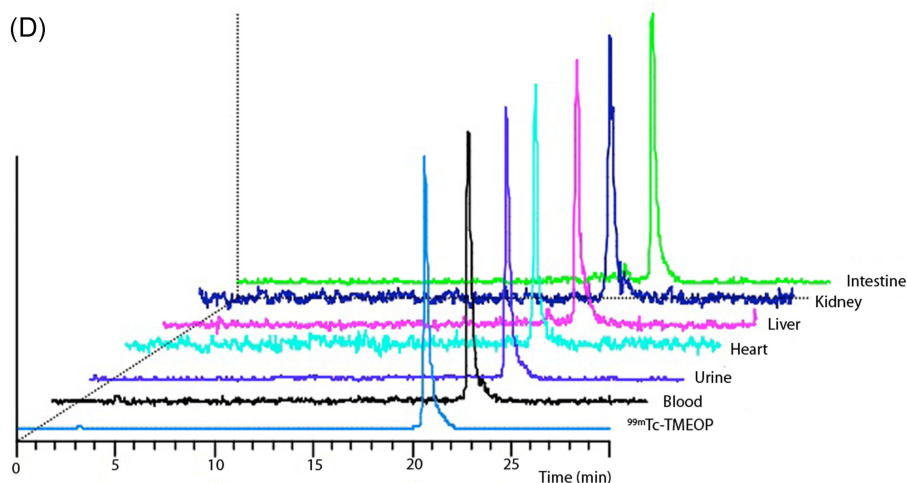


Figure 1. (Continued)

imaging or imaging at a later time point reduces the liver signal, but results can vary significantly between patients (15–19). Therefore new compounds with fast liver clearance are actively being researched. Recent examples of cationic Tc tracers with improved liver clearance are ^{99m}Tc -N-DBODC5, ^{99m}Tc -N-15C5 and ^{99m}Tc -N-MPO (20–22). These complexes contain ^{99m}Tc triple bonded to nitrogen, bisphosphine ligands or ether groups to optimize biodistribution. Neutrally charged ^{99m}Tc complexes such as ^{99m}Tc -teboroxime and ^{99m}Tc -N-NOET have also been developed, demonstrating better flow-extraction properties at high flow rates compared with cationic agents and exhibiting complete redistribution, similar to ^{201}Tl . They show rapid liver clearance, but unfortunately also very rapid myocardial clearance kinetics, limiting their clinical use with the current SPECT technology (23–25).

Here we present a new compound based on tri-carbonyl chemistry. Using tris(pyrazolyl) methane ^{99m}Tc -organometallic complexes as a lead structure we developed tri-methoxy-tris-pyrazolyl- ^{99m}Tc -(CO) $_3$ (^{99m}Tc -TMEOP) (26,27). TMEOP is a neutral and tridentate nitrogen donor chelator that, upon reaction with the organometallic precursor *fac*-[$^{99m}\text{Tc}(\text{OH})_2(\text{CO})_3$] $^+$, forms a moderately lipophilic cationic complex (Fig. 1A) (27). The aim of our study was to evaluate the *in vitro* characteristics and *in vivo* pharmacokinetics of this new candidate for myocardial perfusion imaging in comparison with ^{99m}Tc -sestamibi and ^{99m}Tc -tetrofosmin.

2. MATERIALS AND METHODS

2.1. Synthesis of ^{99m}Tc -TMEOP

One milliliter of a [$^{99m}\text{Tc}(\text{H}_2\text{O})_3(\text{CO})_3$] $^+$ solution (pH 4), obtained using an IsoLink[®] kit (Mallinckrodt Medical BV, the Netherlands), was added to 3.4 mg TMEOP ligand in 80 μl of ethanol. The solution was heated to 100°C for 45 min. After cooling, the pH was adjusted to 7.4 using 1 M NaOH. The labeled compound was analyzed by RP-HPLC using a Nucleosil C $_{18}$ column (10 μm , 250 \times 4 mm) and a gradient of 0.1% TFA and acetonitrile at a flow rate of 1 ml/min. ^{99m}Tc -sestamibi (Cardiolite, Bristol-Myers-Squibb) and ^{99m}Tc -tetrofosmin (Myoview, GE Healthcare) were prepared according to the manufacturer's instructions. Ethanol was added to ^{99m}Tc -sestamibi and ^{99m}Tc -tetrofosmin preparations in order to

obtain the same amount of ethanol injected as compared with ^{99m}Tc -TMEOP injections.

The log $P_{o/w}$ value of ^{99m}Tc -TMEOP was determined under physiological conditions (*n*-octanol–0.1 M PBS, pH 7.4), by the multiple back-extraction method (28).

2.2. In vitro stability and protein binding

The *in vitro* stability of ^{99m}Tc -TMEOP was studied in 0.1 M PBS, pH = 7.4 (37°C, 1 and 24 h incubation) and in human serum and its protein binding was determined. In serum, 100 μl of ^{99m}Tc -TMEOP was added to 900 μl of human serum and incubated at 37°C. Aliquots were taken at 5, 30, 60 and 120 min of incubation and analyzed by RP-HPLC using simultaneous radioactive and UV detection to assess the stability and the protein binding affinity of ^{99m}Tc -TMEOP. The following conditions were applied for RP-HPLC chromatography: Supelguard LC-3DP column (2 cm, 5 μm , Supelco); flow rate = 1 ml/min; gamma and UV detection at 220 nm; eluent A = isopropanol–TFA 0.1% (10:90); eluent B = isopropanol–TFA 0.1% (90:10); gradient: 0–15 min, 95–40% A; 15–20 min 40% A; 20–22 min 40–95% A; 22–30 min 95% A.

2.3. In vivo stability

Sprague–Dawley rats ($n = 4$) were anesthetized using isoflurane and injected intravenously with 100 μl of ^{99m}Tc -TMEOP (7–20 MBq). Animals were sacrificed at 60 min post injection (p.i.) and samples of heart, liver, kidney, blood, urine and intestinal content were collected. Blood was immediately centrifuged for 15 min at 2000 rpm and 4°C and the serum separated. Aliquots of 100 μl of serum were treated with 200 μl of ethanol in order to precipitate the proteins. Samples were cooled at 4°C and centrifuged at 3000 rpm for 15 min. Supernatant was collected and analyzed by RP-HPLC. Heart, liver and kidney samples were rapidly rinsed and placed in cold homogenization buffer (50 mM Tris–0.2 M sucrose buffer, pH = 7.4). Homogenization was performed using a polytron homogenizer. Aliquots (in duplicate) of the liver and kidney homogenates were treated with ethanol (2:1 EtOH–aliquot ratio). The samples were then centrifuged at 15 000 rpm for 15 min at 4°C and the supernatant was analyzed

by RP-HPLC. Urine was centrifuged for 15 min at 3000 rpm and then analyzed by RP-HPLC. The intestinal lumen, corresponding to approximately 80% of the intestinal activity, was rinsed with saline. The liquid fraction containing most of the radioactivity was

separated by centrifugation (4000 rpm for 15 min), filtered (0.22 μm Millex filter) and analyzed by HPLC. The residual activity was further extracted with ethanol and an aliquot also analyzed by RP-HPLC. HPLC conditions for *in vivo* stability were those

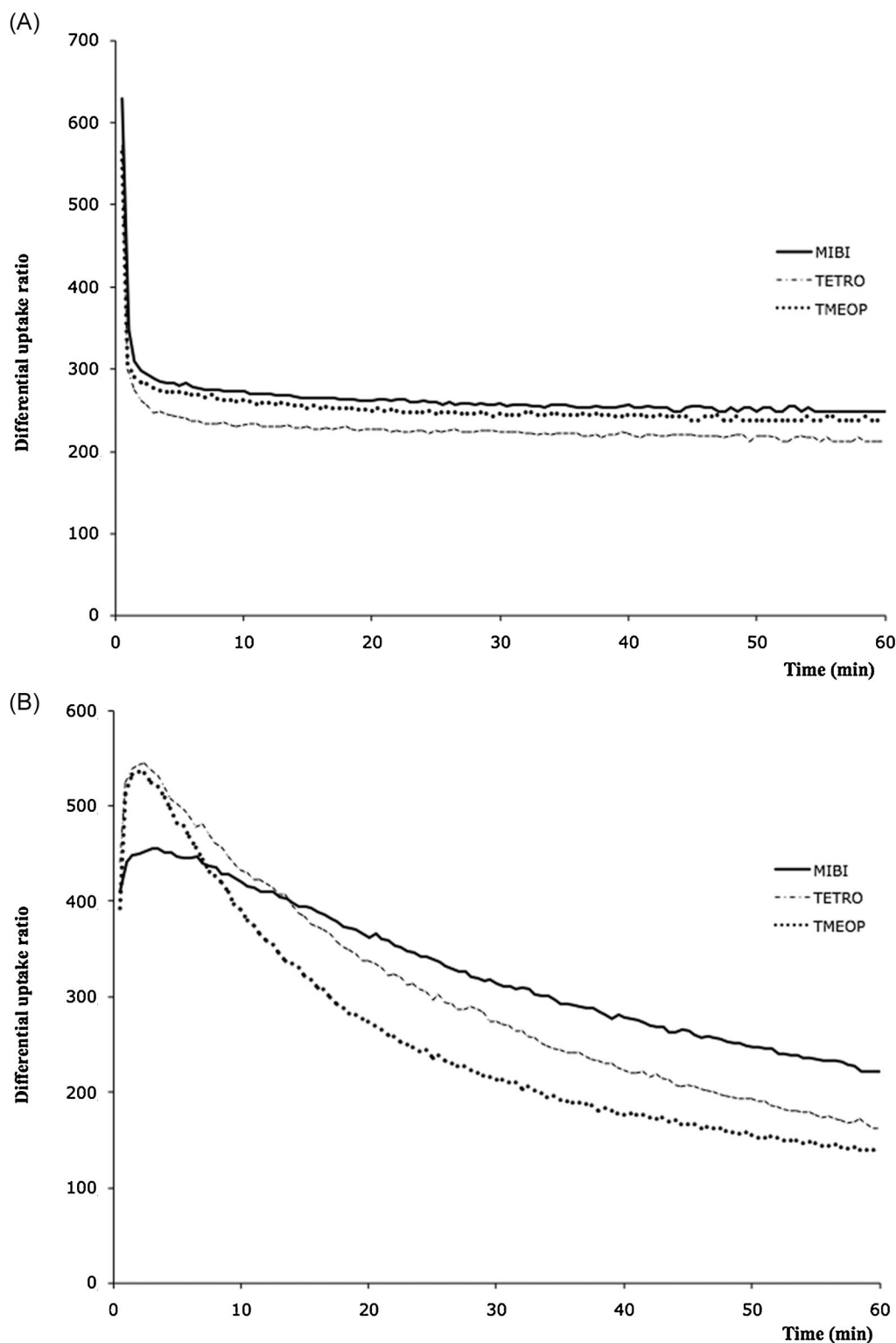


Figure 2. (A) Cardiac uptake of ^{99m}Tc -sestamibi, ^{99m}Tc -tetrofosmin and ^{99m}Tc -TMEOP. (B) Liver uptake of ^{99m}Tc -sestamibi, ^{99m}Tc -tetrofosmin and ^{99m}Tc -TMEOP. (C) Lung uptake of ^{99m}Tc -sestamibi, ^{99m}Tc -tetrofosmin and ^{99m}Tc -TMEOP. Values are averages for six animals. MIBI = ^{99m}Tc -sestamibi; TETRO = ^{99m}Tc -tetrofosmin; TMEOP = ^{99m}Tc -TMEOP.

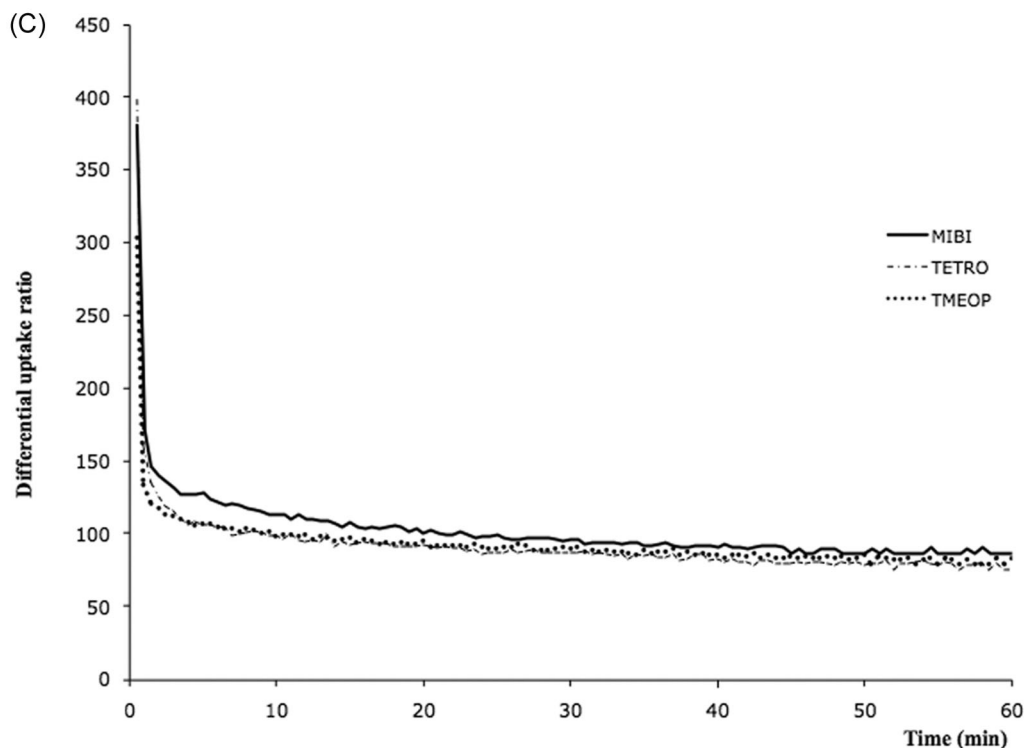


Figure 2. (Contiued)

described for the characterization of ^{99m}Tc -TMEOP. All animal studies were performed with the approval of the local ethical committee for animal research.

2.4. Comparative pharmacokinetic analysis

Pharmacokinetic measurements were performed in healthy male Wistar rats ($n = 18$) aged 5–12 weeks. All animals were allowed free access to food and water. The housing conditions were kept constant throughout the study in order to minimize variations due to physiological parameters. Ten minutes prior to imaging, general anesthesia was induced by isoflurane gas and sustained by intraperitoneal injection of 50 mg/kg pentobarbital. Each animal received an intravenous injection of ± 250 MBq of ^{99m}Tc -TMEOP, ^{99m}Tc -sestamibi or ^{99m}Tc -tetrofosmin ($n = 6$ per tracer) followed by dynamic planar imaging during 1 h. Images were acquired in supine position using one head of a dual-headed gamma camera (e.cam, Siemens Medical Systems,

Malvern, PA, USA) mounted with high-resolution parallel hole collimators (256×256 matrix, zoom 1.76). A total of 410 frames were acquired in two steps: 300 frames of 1 s followed by 110 frames of 30 s. An additional image of 5 min was performed at 2 h p.i. The energy window was set at 20% around 140 keV.

All planar images were processed using AMIDE software (29). Regions of interest (ROIs) were drawn around the entire heart, in the lungs and in the liver. One ROI encompassing the total body was also drawn. All images were analyzed using the same ROIs. Average counts per minute (cpm) were measured for heart, liver and lung in all frames and corrected for injected activity based on the average cpm in the total body ROI for each rat. Time–activity curves were generated for the different ROIs, expressing activity as differential uptake ratio. Curves for heart–liver and heart–lung ratios were calculated as a function of time. Cardiac activity was also expressed as percentage of injected activity (%IA) in the myocardium by dividing the total counts in the ROI encompassing the heart by total counts in the entire body.

Table 1. ^{99m}Tc -TMEOP vs ^{99m}Tc -sestamibi and ^{99m}Tc -tetrofosmin

Total cardiac uptake %IA (mean \pm SD)				
	20 min	40 min	60 min	120 min
^{99m}Tc -TMEOP	1.34 \pm 0.09*	1.31 \pm 0.08*	1.28 \pm 0.06*	1.29 \pm 0.16*
^{99m}Tc -sestamibi	1.42 \pm 0.11*	1.39 \pm 0.11*	1.36 \pm 0.11*	1.26 \pm 0.10*
^{99m}Tc -tetrofosmin	1.21 \pm 0.07	1.20 \pm 0.06	1.16 \pm 0.05	1.11 \pm 0.09

%IA = percentage of injected activity. Data are given as mean values of six rats \pm standard deviation.
* $p < 0.05$ compared with ^{99m}Tc -tetrofosmin, no significance was found between ^{99m}Tc -sestamibi and ^{99m}Tc -TMEOP.

2.5. Cardiac pinhole gated SPECT imaging

Pinhole gated SPECT was performed in a separate group of animals ($n=6$, 3 per tracer). Three animals underwent both ^{99m}Tc -TMEOP and ^{99m}Tc -sestamibi pinhole-gated SPECT imaging. ^{99m}Tc -tetrofosmin imaging was performed in three different rats. Animals were anesthetized and injected with the appropriate

tracer as mentioned above and standard ECG electrodes (3M Health Care, Germany) were taped on three paws. Imaging was performed at 40 min p.i. using the same gamma camera now equipped with pinhole collimators with an aperture of 3 mm (focal length of 250 mm, resulting in a zoom factor of 2). A total of 64 projections of 30 s were acquired over a 360° rotation into a 64×64 matrix. Sixteen time frames were used per cardiac cycle

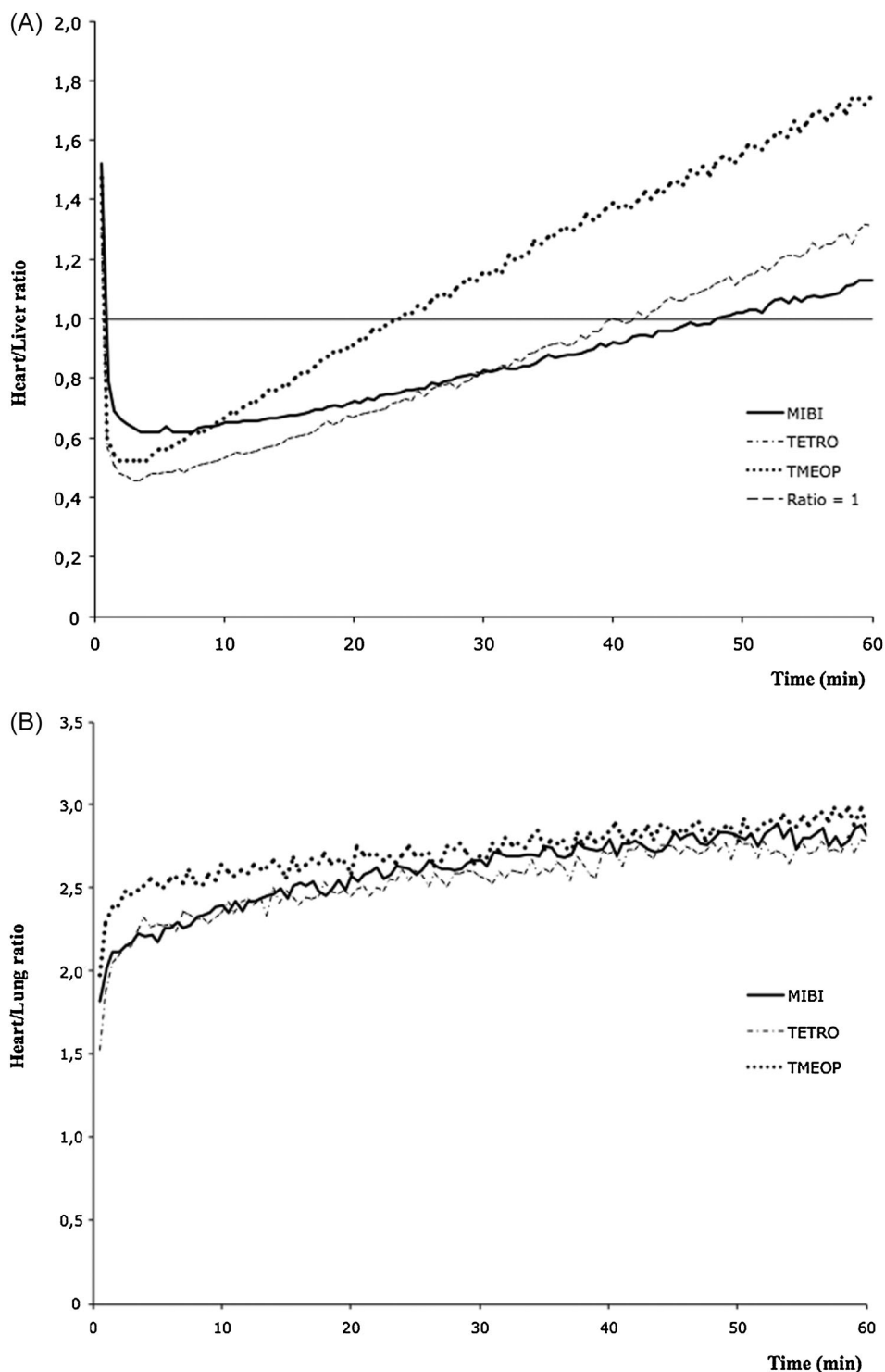


Figure 3. (A) Heart–liver ratio calculated for ^{99m}Tc -sestamibi, ^{99m}Tc -tetrofosmin and ^{99m}Tc -TMEOP. (B) Heart–lung ratio calculated for ^{99m}Tc -sestamibi, ^{99m}Tc -tetrofosmin and ^{99m}Tc -TMEOP. Values are averages for six animals. MIBI = ^{99m}Tc -sestamibi; TETRO = ^{99m}Tc -tetrofosmin; TMEOP = ^{99m}Tc -TMEOP.

and the beat acceptance window was set at the center of the average *R-R* interval calculated just before starting the acquisition. The width of the beat acceptance window was set at 50% of this average *R-R* interval. SPECT images were reconstructed using a modified version of the OSEM algorithm (30). For gated studies the algorithm also includes a smoothness constraint on the temporal properties (31). The images were not corrected for attenuation or scatter. Reconstructed images were further processed using Corridor4DM software for visual analysis of the regional myocardial perfusion and quantitative analysis of the left ventricular volumes and ejection fractions (32). A 3D-ROI was drawn around the left ventricle, using AMIDE, and the average counts per pixel was calculated for all pixels above 50% of the maximum pixel value in the left ventricle. A similar sized 3D-ROI was drawn in the liver for the measurement of the average counts per pixel in the liver. For comparison of the different tracers the heart–liver ratio was calculated by these ROIs.

2.6. Statistical analysis

All data points obtained from planar image analysis were compared between tracers using the non-parametric Man-

n-Whitney *U*-test. Data from the quantitative analysis of ejection fraction, cardiac volumes and heart–liver ratios, as well as the heart–liver ratio on SPECT images were compared between ^{99m}Tc -TMEOP and ^{99m}Tc -sestamibi groups using the Wilcoxon matched pairs signed ranks test, since these observations were paired. Between the ^{99m}Tc -TMEOP and ^{99m}Tc -tetrofosmin and between the ^{99m}Tc -tetrofosmin and ^{99m}Tc -sestamibi groups results were compared using the Mann–Whitney *U*-test. Results were considered significant when *p*-values were less than 0.05.

3. RESULTS

3.1. Radiochemistry, in vitro evaluation and metabolic studies

The complex ^{99m}Tc -TMEOP was obtained in quantitative yield and with high radiochemical purity (>98%) by reacting $[\text{}^{99m}\text{Tc}(\text{H}_2\text{O})_3(\text{CO})_3]^+$ with TMEOP (Fig. 1A). The chemical identity of ^{99m}Tc -TMEOP was established by comparing its HPLC radiochromatogram with the UV–vis trace of the Re surrogate

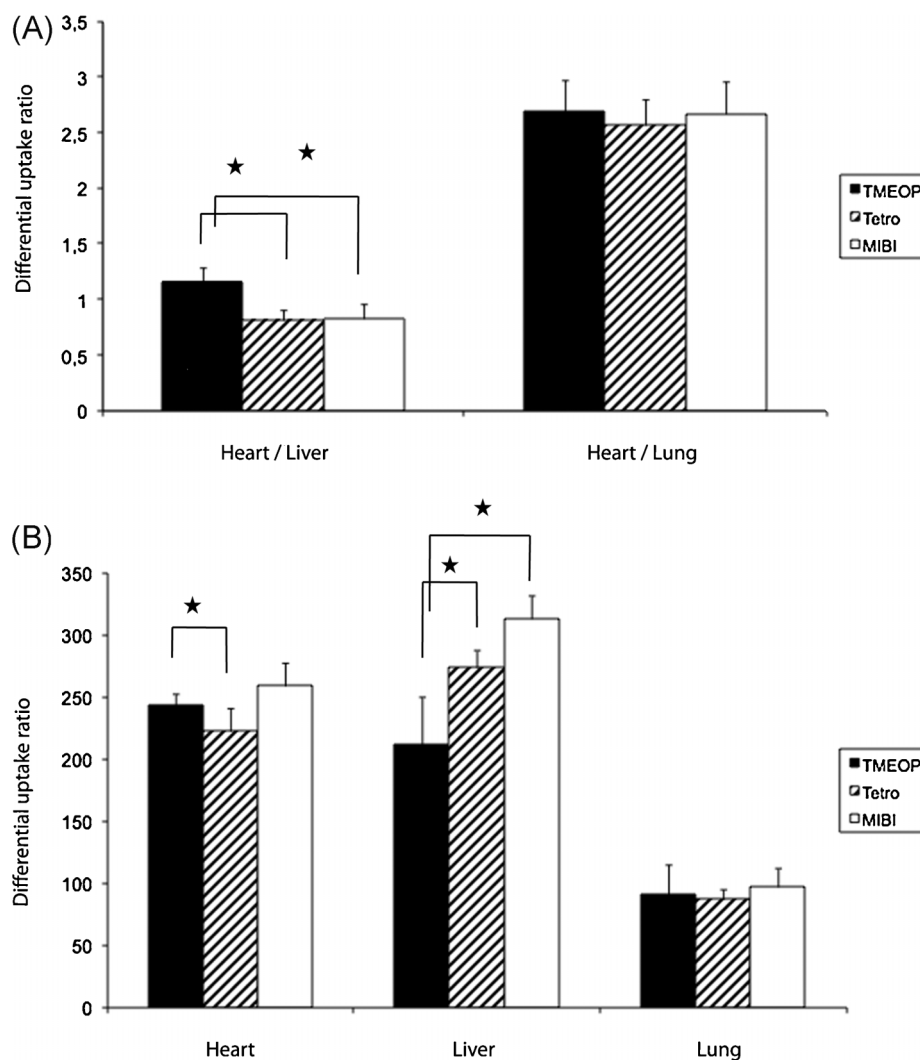


Figure 4. Tracer distribution at clinical time of acquisition (30 min post injection) demonstrating (A) heart–liver and heart–lung ratio for ^{99m}Tc -sestamibi, ^{99m}Tc -tetrofosmin and ^{99m}Tc -TMEOP. (B) Heart, liver and lung uptake for ^{99m}Tc -sestamibi, ^{99m}Tc -tetrofosmin and ^{99m}Tc -TMEOP expressed as differential uptake ratios. Values are averages for six animals. MIBI = ^{99m}Tc -sestamibi; TETRO = ^{99m}Tc -tetrofosmin; TMEOP = ^{99m}Tc -TMEOP. **p* < 0.05.

as shown in Fig. 1(B) (27). ^{99m}Tc -TMEOP is a moderately lipophilic cation that shows a $\log P$ value (0.61 ± 0.04) at the low end of the range considered adequate to have a significant heart uptake and a favorable liver clearance kinetics (33).

^{99m}Tc -TMEOP was stable and did not undergo any transformation, including reoxidation to pertechnetate, even after 24 h of incubation under physiologic conditions, i.e. in 0.1 M PBS (pH 7.4, 37°C) or after 120 min in human serum. The HPLC analysis (gamma and UV detection) of ^{99m}Tc -TMEOP after incubation with human serum did not show any binding to human serum proteins. A representative example of the HPLC analysis of the serum sample after 2 h incubation at 37°C is shown in Fig. 1(C). The chromatogram of ^{99m}Tc -TMEOP after incubation with serum (gamma detection) shows only one radioactive species with the retention time of ^{99m}Tc -TMEOP. No other radioactive species with the retention time of albumin or globulins could be detected. The compound also remained unchanged in all tissue samples at 1 and 2 h post injection (Fig. 1D).

3.2. Pharmacokinetic analysis of ^{99m}Tc -TMEOP

The cardiac, lung and liver time activity curves are shown in Fig. 2. The %IA in the heart at selected time points is shown in Table 1, illustrating the stationary nature of the tracer in the heart over a 2 h interval. Cardiac accumulation was significantly higher ($p < 0.05$) for ^{99m}Tc -TMEOP compared with ^{99m}Tc -tetrofosmin starting at 5 min p.i. and slightly lower compared with ^{99m}Tc -sestamibi (not significant) (Fig. 2A).

Liver activity was significantly lower for ^{99m}Tc -TMEOP compared with both ^{99m}Tc -tetrofosmin ($p < 0.05$ between 16.5 and 40.5 min) and ^{99m}Tc -sestamibi ($p < 0.05$ from 16 min) (Fig. 2B). The liver activity was also significantly lower for ^{99m}Tc -tetrofosmin than for ^{99m}Tc -sestamibi (starting from 25.5 min p.i.; Fig. 2B).

^{99m}Tc -TMEOP demonstrated the lowest initial pulmonary uptake, but later on positioned itself between ^{99m}Tc -sestamibi and ^{99m}Tc -tetrofosmin. However these differences did not reach statistical significance (Fig. 2C).

The heart–liver ratio was significantly higher for ^{99m}Tc -TMEOP compared with ^{99m}Tc -tetrofosmin (from 5 min) and ^{99m}Tc -sestamibi (from 16.5 min p.i.). The heart–liver ratio was higher for ^{99m}Tc -sestamibi than for ^{99m}Tc -tetrofosmin over the first 14.5 min after tracer administration (Fig. 3A). There were no important differences in heart–lung ratio (Fig. 3B).

Figure 4 compares the distribution of ^{99m}Tc -TMEOP in heart, liver and lung tissue and the derived heart–liver and heart–lung ratios at the time of acquisition normally applied in clinical settings, i.e. 30 min after injection between ^{99m}Tc -TMEOP, ^{99m}Tc -sestamibi and ^{99m}Tc -tetrofosmin. This confirms the significantly higher heart–liver ratio in the ^{99m}Tc -TMEOP group compared with the other tracers. Summed images illustrating the total body distribution of the tracers between 30 to 35 minutes after injection and a 5 min image at 2 h after injection are shown in Fig. 5.

3.3. Cardiac pinhole-gated SPECT imaging

Figure 6 shows representative non-gated SPECT images for ^{99m}Tc -sestamibi, ^{99m}Tc -tetrofosmin and ^{99m}Tc -TMEOP. The quality

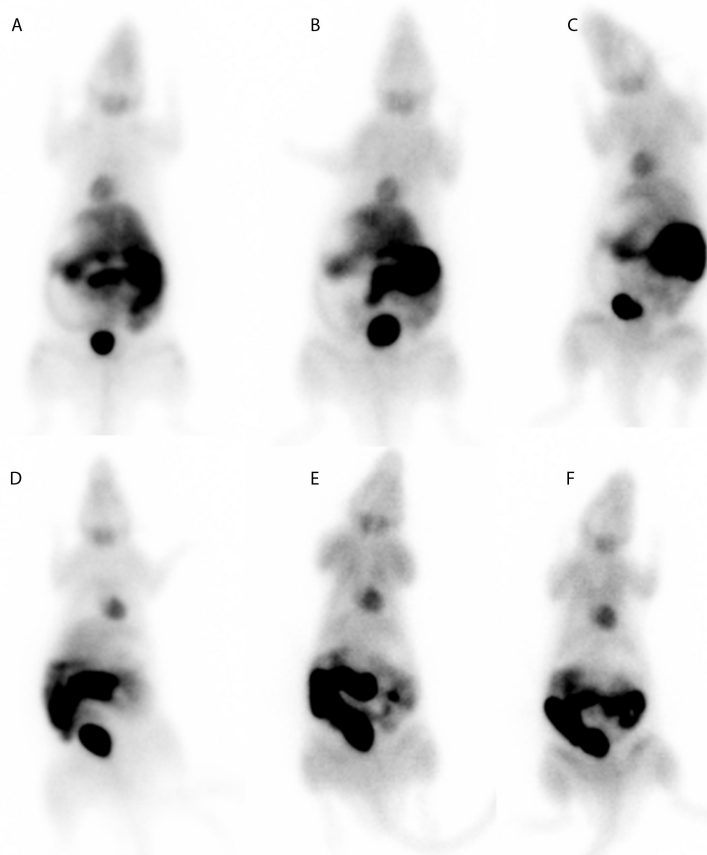


Figure 5. Summed planar whole body images of frames 350–360, 30–35 min post injection with (A) ^{99m}Tc -sestamibi; (B) ^{99m}Tc -tetrofosmin; (C) ^{99m}Tc -TMEOP and late images representing 5 min acquisition 2 h post injection with (D) ^{99m}Tc -sestamibi, (E) ^{99m}Tc -tetrofosmin; and (F) ^{99m}Tc -TMEOP.

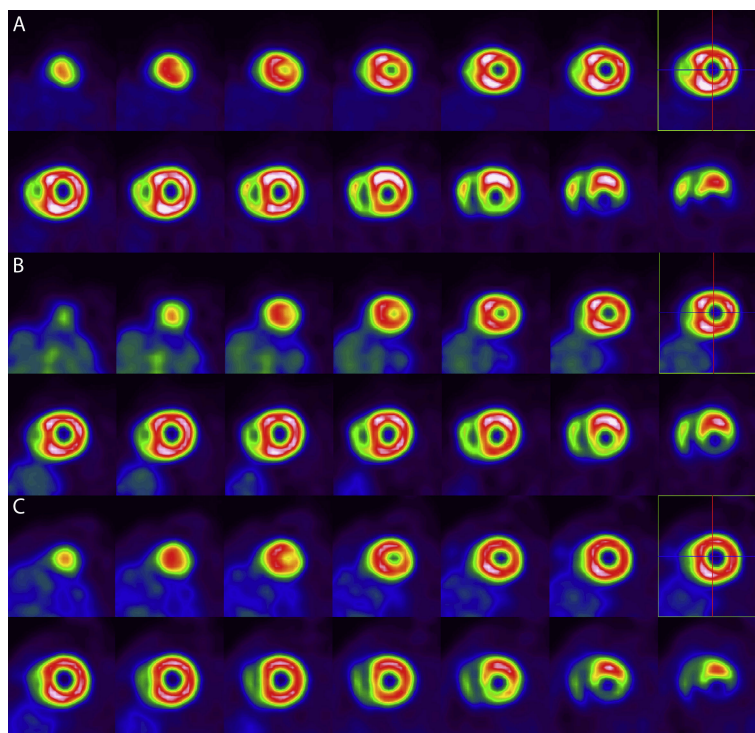


Figure 6. Representative SPECT image analysis at 40 minutes after administration: short axis slices representing (A) ^{99m}Tc -TMEOP; (B) ^{99m}Tc -sestamibi and (C) ^{99m}Tc -tetrofosmin.

of the left ventricular perfusion images obtained with ^{99m}Tc -TMEOP is high and comparable to ^{99m}Tc -sestamibi and ^{99m}Tc -tetrofosmin images. All images showed a homogeneous perfusion in the left ventricular wall. The heart–liver ratio was comparable for ^{99m}Tc -sestamibi and ^{99m}Tc -tetrofosmin but two times higher for ^{99m}Tc -TMEOP (Table 2).

The functional parameters obtained from the gated data were comparable for all tracers. The differences between ^{99m}Tc -TMEOP and ^{99m}Tc -sestamibi or ^{99m}Tc -tetrofosmin never reached statistical significance (Table 2).

4. DISCUSSION

^{99m}Tc -sestamibi and ^{99m}Tc -tetrofosmin are widely applied as myocardial perfusion tracers in nuclear medicine for the detection of coronary artery disease and myocardial viability.

Although presenting adequate radiochemical characteristics, they suffer from high and prolonged liver or gastro-intestinal retention (4–9). This limits the diagnostic accuracy of myocardial perfusion SPECT using these tracers, especially for the evaluation of the perfusion in the inferior and infero-apical wall.

Here we introduce ^{99m}Tc -TMEOP as a new compound, based on tricarbonyl chemistry for myocardial perfusion imaging. In rats it shows cardiac uptake comparable to ^{99m}Tc -sestamibi and ^{99m}Tc -tetrofosmin, but significantly faster liver clearance. At 40 min p.i. the heart–liver ratio of ^{99m}Tc -TMEOP, derived from the SPECT data, is twice that of ^{99m}Tc -sestamibi and ^{99m}Tc -tetrofosmin. These results are comparable to the 30 min values published for ^{99m}Tc -N-DBODC5 (6.01 ± 1.45) (21), but inferior to the data reported for ^{99m}Tc -N-MPO (12.75 ± 3.34) (22).

The heart uptake of cationic radiotracers and the factors governing their liver clearance kinetics are not fully understood. However, several mechanistic studies suggest that molecular size,

Table 2. ^{99m}Tc -TMEOP vs ^{99m}Tc -sestamibi and ^{99m}Tc -tetrofosmin

Pinhole gated SPECT comparison (mean \pm SD)				
	Heart–liver ratio	EDV (ml)	ESV (ml)	EF (%)
^{99m}Tc -TMEOP	6.98 ± 1.66	0.39 ± 0.06	0.12 ± 0.03	70.7 ± 3.5
^{99m}Tc -sestamibi	2.48 ± 0.30	0.39 ± 0.04	0.11 ± 0.02	72 ± 2.6
^{99m}Tc -tetrofosmin	2.66 ± 0.40	0.38 ± 0.05	0.11 ± 0.03	70 ± 2.6

EDV = end diastolic volume; ESV = end systolic volume; EF = ejection fraction. Data are given as mean values of three rats \pm standard deviation.

lipophilicity and charge play a major role in the uptake and retention in myocytes (21,34,35). In particular, ether containing chelators has been used to prepare complexes with improved heart-background ratios (36). The lipophilicity modulates the entry into the sarcolemmal and mitochondrial membranes, while the negative mitochondrial potential provides the electrochemical driving force for the radiotracers to enter the myocytes mitochondria (37–41). As the myocardium has an increased mitochondrial population compared with normal tissue, lipophilic cationic radiotracers, such as ^{99m}Tc-Sestamibi and ^{99m}Tc-tetrofosmin, tend to localize in heart (42,43). This accumulation is also visible in other mitochondrion-rich organs, such as liver, kidneys and salivary gland. We assume that this mechanism is also valid for ^{99m}Tc-TMEOP. Molecular size and charge of ^{99m}Tc-TMEOP is comparable to both ^{99m}Tc-sestamibi and ^{99m}Tc-tetrofosmin. The log*P* of ^{99m}Tc-TMEOP is relatively low compared with that of ^{99m}Tc-sestamibi: 0.61 ± 0.04 vs 1.29 ± 0.15 (44). However, total cardiac uptake in our study is similar to that of ^{99m}Tc-sestamibi. Subtle differences in cardiac uptake between tracers might not be detectable in healthy rats because of the high coronary flow rate in these animals. Uptake is closely related to flow but at higher flow rates there is no linear relationship between flow and extraction for most perfusion tracers. The determination of the flow-extraction curve is an important parameter for any new cardiac perfusion tracer because it will determine the sensitivity for detecting cardiac ischemia. This type of analysis is best performed in larger animal species that have lower coronary flow rates comparable to humans. Such analysis was beyond the scope of the current study.

The metabolite studies performed for ^{99m}Tc-TMEOP have shown that this complex does not undergo any metabolic transformation in rats. Therefore, the faster liver washout of TMEOP is not due to its transformation into more hydrophilic and more easily excreted metabolites. We hypothesize that the faster liver washout is mainly related to the lower lipophilicity of the compound.

Assuming that the differences in pharmacokinetic properties can be translated to humans makes ^{99m}Tc-TMEOP a very attractive alternative for myocardial perfusion imaging. The use of this type of tracer, which allows imaging quickly after injection, is in accordance with the other recent developments in nuclear cardiology such as selective adenosine agonists and the clinical use of dedicated solid-state SPECT cameras (45,46). Rapidly clearing tracers, short pharmacological stress protocols and ultra-fast image acquisitions all contribute significantly to better patient care and now allow for high-throughput screening of patients at risk for cardiac ischemia, further establishing the role of gated perfusion SPECT.

5. CONCLUSION

Based on the tricarbonyl technology, we have introduced a novel moderately lipophilic cation, ^{99m}Tc-TMEOP, which appears to be a good candidate for further evaluation in larger animals and eventually in humans as a myocardial perfusion agent. ^{99m}Tc-TMEOP is a highly stable complex that is not metabolized in rat. The favorable biodistribution of ^{99m}Tc-TMEOP might enable high-quality cardiac imaging early after tracer injection, thereby reducing the duration of the cardiac imaging protocol. The liver washout kinetics of ^{99m}Tc-TMEOP suggests that photon scatter from the liver into the inferior and infero-apical walls on

myocardial perfusion images will not be a problem using ^{99m}Tc-TMEOP. This should result in fewer artifacts and improved diagnostic accuracy for detecting coronary artery disease compared with both ^{99m}Tc-sestamibi and ^{99m}Tc-tetrofosmin.

Acknowledgements

The financial support of Mallinckrodt Med. BV, Petten, The Netherlands to ITN is acknowledged. Matthias Bauwens, Hector Knight and Geert Ensing are acknowledged for their cooperation in labeling and production of ^{99m}Tc-TMEOP. Lode Goethals is a Ph.D. fellow of the Research Foundation Flanders. Tony Lahoutte is a Senior Clinical Investigator of the Research Foundation, Flanders. The research at ICMI is funded by the Interuniversity Attraction Poles Programme, Belgian State, Belgian Science Policy.

References

- Beller GA, Watson DD. Physiological basis of myocardial perfusion imaging with the technetium 99m agents. *Semin Nucl Med* 1991; 21: 173–181.
- Kelly JD, Forster AM, Higley B, et al. Technetium-99m-tetrofosmin as a new radiopharmaceutical for myocardial perfusion imaging. *J Nucl Med* 1993; 34: 222–227.
- Nakajima K, Taki J, Shuke N, Bunko H, Takata S, Hisada K. Myocardial perfusion imaging and dynamic analysis with technetium-99m tetrofosmin. *J Nucl Med* 1993; 34: 1478–1484.
- Parker JA. Cardiac nuclear medicine in monitoring patients with coronary heart disease. *Semin Nucl Med* 2001; 31: 223–237.
- Kapur A, Latus KA, Davies G, Dhawan RT, Eastick S, Jarritt PH, et al. A comparison of three radionuclide myocardial perfusion tracers in clinical practice: the ROBUST study. *Eur J Nucl Med* 2002; 29: 1608–1616.
- Kailasnath P, Sinusas AJ. Comparison of TI-201 with Tc-99m labeled myocardial perfusion agents: technical, physiological, and clinic issues. *J Nucl Cardiol* 2001; 8: 482–498.
- Llaurado JG. The quest for the perfect myocardial perfusion indicator. still a long way to go. *J Nucl Med* 2001; 42: 282–284.
- Germano G, Chua T, Kiat H, Areeda JS, Berman DS. A quantitative phantom analysis of artifacts due to hepatic activity in technetium-99m myocardial perfusion SPECT studies. *J Nucl Med* 1994; 35: 356–359.
- Nuyts J, Dupont P, Van den Maegdenbergh V, Vleugels S, Suetens P, Mortelmans L. Study of the liver-heart artifact in emission tomography. *J Nucl Med* 1995; 36: 133–139.
- Heller GV. Tracer selection with different stress modalities based on tracer kinetics. *J Nucl Cardiol* 1996; 5: S15–S21.
- Glover DK, Ruiz M, Yang JY, Smith WH, Watson DD, Beller GA. Myocardial Tc-99m tetrofosmin uptake during adenosine induced vasodilatation with either a critical or mild coronary stenosis. Comparison with TI-201 and regional myocardial blood flow. *Circulation* 1997; 96: 2332–2338.
- Watson DD, Glover DK. Overview of kinetics and modelling. In *Nuclear Cardiology: State of the Art and Future Directions*, Zaret BL, Beller GA (eds). Mosby: St Louis, MO, 1993; 3–12.
- Shanoudy H, Raggi P, Beller GA, et al. Comparison of technetium-99m tetrofosmin and thallium-201 single-photon emission computed tomographic imaging for detection of myocardial perfusion defects in patients with coronary artery disease. *J Am Coll Cardiol* 1998; 31: 331–337.
- Higley B, Smith FW, Smith T, et al. Technetium-99m-1,2 [bis(2-ethoxyethyl) phosphino]ethane: human biodistribution, dosimetry and safety of a new myocardial perfusion imaging agent. *J Nucl Med* 1993; 34: 30–38.
- Banerjee S, Pillai MRA, Ramamoorthy N. Evolution of Tc-99m in diagnostic radiopharmaceuticals. *Semin Nucl Med* 2001; 31: 260–277.
- Boz A, Gungor F, Karayalcin B, Yildiz A. The effects of solid food in prevention of intestinal activity in Tc-99m tetrofosmin myocardial perfusion scintigraphy. *J Nucl Cardiol* 2003; 10: 161–167.

17. van Dongen AJ, van Rijk PP. Minimizing liver, bowel, and gastric activity in myocardial perfusion SPECT. *J Nucl Med* 2000; 41: 1315–1317.
18. Hurwitz GA, Clark EM, Slomka PJ, Siddiq SK. Investigation of measures to reduce interfering abdominal activity on rest myocardial images with Tc-99m sestamibi. *Clin Nucl Med* 1993; 18: 735–741.
19. Boz A, Karayalcin B. Which is better for inferior wall evaluation: a full or empty stomach? *J Nucl Med* 1996; 37: 1916–1917.
20. Hatada K, Riou LM, Ruiz M, et al. 99mTc-N-DBODCS, a new myocardial perfusion imaging agent with rapid liver clearance: comparison with 99mTc-sestamibi and 99mTc-tetrofosmin in rats. *J Nucl Med* 2004; 45: 2095–2101.
21. Liu S, He ZJ, Hsieh WY, Kim YS. Evaluation of novel cationic 99mTc-nitrido complexes as radiopharmaceuticals for heart imaging: improving liver clearance with crown ether groups. *Nucl Med Biol* 2006; 33: 419–432.
22. Kim YS, Wang J, Broisat A, Glover DK, Liu S. Tc-99m-N-MPO: novel cationic Tc-99m radiotracer for myocardial perfusion imaging. *J Nucl Cardiol* 2008; 15: 535–546.
23. Pasqualini R, Duatti A, Bellande E, et al. Bis (dithiocarbamate) nitrido technetium-99m radiopharmaceuticals: a class of neutral myocardial imaging agents. *J Nucl Med* 1994; 35: 334–341.
24. Fagret D, Ghezzi C, Vanzetto G. 99mTc-N-NOET imaging for myocardial perfusion: can it offer more than we already have? *J Nucl Med* 2001; 42: 1395–1396.
25. Leppo JA, DePuey EG, Johnson LL. A review of cardiac imaging with sestamibi and teboroxime. *J Nucl Med* 1991; 32: 2012–2022.
26. Maria L, Cunha S, Videira M, et al. Rhenium and technetium tricarbonyl complexes anchored by pyrazole-based tripods: novel lead structures for the design of myocardial imaging agents. *Dalton Trans* 2007; 3010–3019.
27. Maria L, Fernandes C, Garcia R, et al. Tris(pyrazolyl)methane 99mTc tricarbonyl complexes for myocardial imaging. *Dalton Trans* 2009; 603–606.
28. Troutner DE, Volkert WA, Hoffman TJ, Holmes RA. A neutral lipophilic complex of ^{99m}Tc with a multidentate amine oxime. *Int J Appl Radiat Isot* 1984; 35: 467–470.
29. Loening AM, Gambhir SS. AMIDE: a free software tool for multimodality medical image analysis. *Mol Imag* 2003; 2: 131–137.
30. Vanhove C, et al. Interest of the ordered subsets expectation maximization (OS-EM) algorithm in pinhole single-photon emission tomography reconstruction: a phantom study. *Eur J Nucl Med* 2000; 27: 140–146.
31. Vanhove C, et al. Reconstruction of gated myocardial perfusion SPET incorporating temporal information during iterative reconstruction. *Eur J Nucl Med Mol Imag* 2002; 29: 465–472.
32. Ficaro EP, Lee BC, Kritzman JN, Corbett JR. Corridor 4DM: the Michigan method for quantitative nuclear cardiology. *J Nucl Cardiol* 2007; 14: 455–465.
33. Liu S. Ether and crown ether-containing cationic ^{99m}Tc complexes useful as radiopharmaceuticals for heart imaging. *Dalton Trans* 2007; 1183–1193.
34. Kim YS, He ZJ, Hseh WY, Liu S. Synthesis, characterization and X ray crystal structure of [Re(PNP)(CO)₃]Br·2CH₃OH: model compound for a new class of cationic 99mTc radiotracers. *Inorg Chem Acta* 2006; 359: 2479–2488.
35. Carvalho PA, Chiu ML, Kronauge JF, et al. Subcellular distribution and analysis of Technetium-99m-MIBI in isolated perfused rat hearts. *J Nucl Med* 1992; 33: 1516–1522.
36. Marmion ME, Woulfe SR, Neumann WL, Nosco DL, Deutsch E. Preparation and characterization of technetium complexes with Schiff-base and phosphine coordination. 1. Complexes of technetium-99g and -99m with acac₂en and trialkyl phosphines (where acac₂en=N,N'-ethylenebis[acetylacetonate iminato]). *Nucl Med Biol* 1999; 26: 755–770.
37. Deutsch E, Ketring AR, Libson K, Vanderheyden J, Hirth WW. The Noah's ark experiment: Species dependent biodistributions of cationic 99mTc complexes. *Nucl Med Biol* 1989; 16: 191–232.
38. Platts EA, North TL, Pickett RD, Kelly JD. Mechanism of uptake of technetium-tetrofosmin. I: uptake into isolated adult rat ventricular myocytes and subcellular localization. *J Nucl Cardiol* 1995; 2: 317–326.
39. Younes A, Songadele JA, Maublant J, Platts E, Pickett R, Veyre A. Mechanism of uptake of technetium-tetrofosmin. II: uptake into isolated adult rat heart mitochondria. *J Nucl Cardiol* 1995; 2: 327–333.
40. Bolzati C, Uccelli L, Boschi A, et al. Synthesis of a novel class of nitrido Tc-99m radiopharmaceuticals with phosphino-thiol ligands showing transient heart uptake. *Nucl Med Biol* 2000; 27: 369–374.
41. Piwnicka-Worms D, Kronauge FP, Chiu ML. Uptake and retention of hexakis (2-methoxyisobutyl isonitrile) technetium (I) in cultured chick myocardial cells. Mitochondrial and plasma membrane potential dependence. *Circulation* 1990; 82: 1826–1832.
42. Duchon MR. Mitochondria in health and disease: perspectives on a new mitochondrial biology. *Mol Asp Med* 2004; 25: 365–451.
43. Kim YS, Shi J, Zhai S, Hou G, Liu S. Mechanism for myocardial localization and rapid liver clearance of Tc-99m-N-MPO: a new perfusion radiotracer for heart imaging. *J Nucl Cardiol* 2009; 16: 571–579.
44. Liu S, He ZJ, Hsieh WY, Kim YS. Impact of bidentate chelators on lipophilicity, stability and biodistribution characteristics of cationic 99mTc-nitrido complexes. *Bioconj Chem* 2007; 18: 929–936.
45. Hendel RC, Jamil T, Glover DK. Pharmacologic stress testing: new methods and new agents. *J Nucl Cardiol* 2003; 2: 197–204.
46. Esteves FP, Raggi P, Folks RD, et al. Novel solid-state-detector dedicated cardiac camera for fast myocardial perfusion imaging: multicenter comparison with standard dual detector cameras. *J Nucl Cardiol* 2009; 16: 927–934.